HYDROLOGICAL PROCESSES
Hydrol. Process. **15**, 337–358 (2001)

Erosion prediction on unpaved mountain roads in northern Thailand: validation of dynamic erodibility modelling using KINEROS2

Alan D. Ziegler,* Thomas W. Giambelluca and Ross A. Sutherland
University of Hawaii at Manoa, Department of Geography, 55B 445, 2424 Maile Way, Honolulu, Hawaii 96822, USA

Abstract:

The event- and physics-based KINEROS2 runoff/erosion model for predicting overland flow generation and sediment production was applied to unpaved mountain roads. Field rainfall simulations conducted in northern Thailand provided independent data for model calibration and validation. Validation shows that KINEROS2 can be parameterized to simulate total discharge, sediment transport and sediment concentration on small-scale road plots, for a range of slopes, during simulated rainfall events. The KINEROS2 model, however, did not accurately predict time-dependent changes in sediment output and concentration. In particular, early flush peaks and the temporal decay in sediment output were not predicted, owing to the inability of KINEROS2 to model removal of a surface sediment layer of finite depth. After 15–20 min, sediment transport declines as the supply of loose superficial material becomes depleted. Modelled erosion response was improved by allowing road erodibility to vary during an event. Changing the model values of erosion detachment parameters in response to changes in surface sediment availability improved model accuracy of predicted sediment transport by 30–40%. A predictive relationship between road erodibility 'states' and road surface sediment depth is presented. This relationship allows implementation of the dynamic erodibility (DE) method to events where pre-storm sediment depth can be estimated (e.g., from traffic usage variables). Copyright © 2001 John Wiley & Sons, Ltd.

KEY WORDS road erosion modelling; model validation; runoff generation; erodibility

INTRODUCTION

Roads and road-building disrupt watershed hydrological and geomorphological systems and contribute to adverse cumulative watershed effects (Reid, 1993; Montgomery, 1994). In some instances, road impacts may be greater than those of other recognized disruptive activities. Megahan and Ketcheson (1996) state that the primary sediment source from logging activities in western USA is forest access roads, rather than other timber management activities (e.g. Megahan and Kidd, 1972). In a field study near Melbourne, Australia Grayson *et al*. (1993) determined that timber harvesting activities did not greatly affect stream physical and chemical water quality, but improperly placed or maintained roads contributed substantial sediment quantities. In mountainous northern Thailand, we have demonstrated that unpaved rural roads can disrupt hydrological and erosional processes disproportionately to their areal extent, compared with agriculture-related lands (Ziegler and Giambelluca, 1997a,b). Despite evidence that road-related impacts often outweigh those of other activities, conservation efforts historically have focused on agricultural and timber removal activities. In an attempt to better understand road impacts, geomorphologists and hydrologists have been approaching the goal of modelling road-related physical processes realistically (e.g. Simons *et al*., 1977, 1978; Ward and Seiger, 1983; Flerchinger and Watts, 1987; Luce and Cundy, 1994; Elliot *et al*., 1995; Anderson and MacDonald, 1998;

* Correspondence to: Dr Alan Ziegler, University of Hawaii at Manoa, Department of Geography, 55B 445, 2424 Maile Way, Honolulu, Hawaii 96822, USA. E-mail: adz@hawaii.edu

Received 28 October 1999
Accepted 21 March 2000

Storck *et al*., 1998). Physically based models are potentially important tools in the labour-intensive, time-consuming process of investigating how roads disrupt basin hydrological and erosional processes, provided that:

1. model equations describe underlying runoff generation and erosion processes realistically;
2. necessary parameters and datasets can be obtained for the model;
3. calibration and validation is performed to ensure the model accuracy.

Herein, we test the use of the KINEROS2 model for predicting road runoff and erosion on an unpaved road in the Pang Khum Experimental Watershed (PKEW) in northern Thailand, the site of our ongoing investigation of road-related impacts in montane mainland southeast Asia (Ziegler *et al*., 2000a, b; in press).

THE KINEROS2 MODEL

KINEROS2 (Smith *et al*., 1995), the second-generation version of KINEROS (Woolhiser *et al*., 1990), is an event-based, physics-based runoff and erosion model. Application and testing of KINEROS is documented elsewhere (Smith, 1976; Smith *et al*., 1995). Dynamic, distributed flow modelling in KINEROS2 is well-suited to describe road runoff and erosion processes in PKEW, where:

1. runoff generation on roads is dominated by the Horton overland flow (HOF) mechanism, with minimal contributions from return flow;
2. sediment transport on the road surface varies throughout the course of a storm.

The following description of KINEROS2 is based on Smith *et al*. (1995) and C. Unkrich (unpublished manuscript, Southwest Watershed Research Center, USDA-ARS, Tuscon, AZ).

Horton overland flow simulation in KINEROS2 utilizes the kinematic wave method to solve the dynamic water balance equation

$$\frac{\partial h}{\partial t} + \frac{\partial Q}{\partial x} = q(x, t) \tag{1}$$

where h is water storage per unit area, $Q(x, t)$ is water discharge, x is distance downslope, t is time, and $q(x, t)$ is net lateral inflow rate. Solution of Equation (1) requires estimates of time- and space-dependent rainfall $r(x, t)$ and infiltration $f(x, t)$ rates

$$q(x, t) = r(x, t) - f(x, t) \tag{2}$$

The infiltration model in KINEROS2 utilizes several parameters describing a one- or two-layer soil profile: saturated hydraulic conductivity (K_s), integral capillary drive or matric potential (G), porosity (ϕ), and pore size distribution index (λ). The coefficient of variation for K_s also can be specified to account for spatial variation in infiltration. Inclusion of two soil layers allows the modelling of a restrictive surface or subsurface layer. The general one-layer infiltrability (f_c) model is a function of cumulative infiltration (I)

$$f_c = K_s \left[1 + \frac{\alpha}{e^{(\alpha I/B)} - 1}\right] \tag{3}$$

where α represents soil type (fixed at 0·85) and $B = (G + h_w)(\Theta_s - \Theta_I)$, where h_w is surface water depth and G is net capillary drive; the second term, unit storage capacity, is the difference of effective saturation (Θ_s) and soil moisture (Θ_I).

Simulating erosion involves solving the dynamic sediment mass balance equation

$$\frac{\partial(AC_s)}{\partial t} + \frac{\partial(QC_s)}{\partial x} - e(x,t) = q(x,t)c(x,t) \tag{4}$$

where A is cross-sectional area, C_s is local sediment concentration, e is net erosion/deposition rate, $q(x,t)$ is water inflow rate and $c(x,t)$ is the corresponding concentration of the inflowing water. The KINEROS2 model does not explicitly separate rill and interrill erosion processes (often there are no rills); rather, e is divided into rainsplash (e_s) and net hydraulic erosion (e_h) subcomponents

$$e = e_s + e_h \tag{5}$$

Splash erosion is estimated from the relationship

$$e_s = \begin{cases} c_f k(h) r^2 & q > 0 \\ 0 & q < 0 \end{cases} \tag{6}$$

where r is rainfall intensity, c_f is a constant related to soil erodibility, $k(h)$ is a function of surface water depth that reduces the splash erosion rate as water depth increases, and q is excess rainfall (i.e. rainfall > infiltration + surface ponding). Flow-induced net hydraulic erosion is the difference between particle detachment (dependent on slope, flow depth, flow velocity, particle size) and deposition. In KINEROS2, e_h is calculated as a function of current local sediment concentration $C_s(x,t)$ and transport capacity (C_{mx})

$$e_h = c_g(C_{mx} - C_s)A \tag{7}$$

where A is cross-sectional area of the flowing water and c_g is a transfer rate coefficient, which is equal to soil particle settling velocity (v_s) / hydraulic depth (h) during deposition; and c_g is less than v_s/h during erosion on cohesive soils.

Drainage basins in KINEROS2 are treated as a cascading network of surface, channel and pond elements. Channels receive flow from adjacent surfaces or upslope channels. Rectangular surfaces may be cascaded or arranged in parallel to represent complex topography or erosion features. A road section could be represented as one element or subdivided into parallel flow planes representing distinct features, such as ruts, gullies or tracks. Each element is characterized by assigning parameter values that control runoff generation and erosion processes. Dynamic, distributed flow modelling in KINEROS2 requires a temporal record of rainfall rate at one or more locations.

STUDY AREA

The Pang Khum Experiment Watershed (PKEW) is near Pang Khum village (19°3′N, 98°39′E), within Samoeng District of Chiang Mai Province, about 60 km NNW of Chiang Mai, Thailand (Figure 1). The monsoon rainy season extends from mid-May through to November, during which about 90% of the 1200–1300 mm annual rainfall occurs. Bedrock within the 93·7-ha basin is Triassic granite; PKEW soils are dominantly Ultisols, Alfisols and Inceptisols. Soil properties determined on the Lower PKEW Road are listed in Table I. Roads, access paths and dwelling sites each comprise <1% of the PKEW area. Approximately 12% of the basin area is agricultural land (cultivated, upland fields, and <1·5-year-old abandoned); 13% is comprised of fallow lands (not used for 1·5–4 years); 31 and 12% are young (4–10 years) and advanced secondary vegetation, respectively; and 31% is disturbed, primary forest.

Despite light traffic, the Upper and Lower PKEW Roads are important sediment sources for material entering the stream channel network (Figure 2; Ziegler *et al*., in press). At the beginning of the rainy season, loose road surface material that has accumulated during the dry season is flushed by surface flow during the first few rainstorms. Thereafter, daily traffic detaches more sediment and creates ruts for gully initiation.

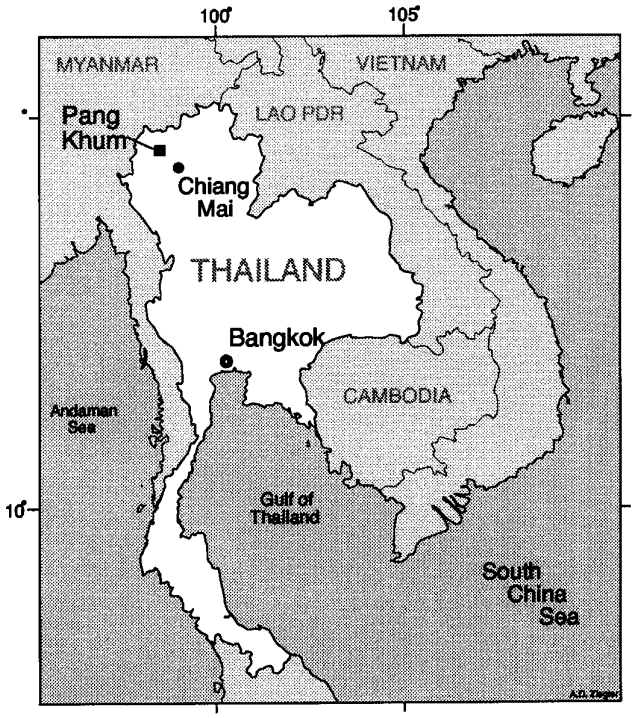

Figure 1. Location of the Pang Khum village in northern Thailand

Filling of gullies with unconsolidated material is an additional source of easily eroded material. Because HOF is frequently generated on roads (Ziegler and Giambelluca, 1997a), surface runoff frequently transports sediment and incises concentrated flow channels during the wet period. Throughout much of the watershed, approximately 75% of all road runoff directly enters the stream network at intersections of the road and stream channel. Because the PKEW roads are not major arteries, we were able to conduct numerous experiments without interrupting daily traffic patterns; additionally we could control usage during experiments investigating vehicle detachment.

METHODS AND MATERIALS

Rainfall simulation

In February 1998 and 1999, rainfall simulation experiments were conducted on the Lower PKEW Road. Eight simulations (ROAD) were conducted on a road section with experimental plot slopes ranging from 0·13 to 0·18 (m m^{-1}). Four simulations were performed on the steepest road section in PKEW (HILL, slope = 0·29 m m^{-1}). One day following the ROAD simulations, an additional simulation was performed on each ROAD plot to investigate sediment transport during successive storms (WET). The rainfall simulator consisted of two vertical, 4·3-m risers, each directing one 60° axial full cone nozzle (70 μm orifice diameter) toward the surface. Water was supplied to the simulator by a 750 W centrifugal pump at 172 kPa (25 p.s.i.). This operating pressure produced rainfall energy flux densities (EFD) ranging from about 1700 to 1900 J m^{-2} h^{-1} (100–115 mm h^{-1}), approximating energies sustained for 10–20 min during the largest annual PKEW storms (based on preliminary analysis of 2 years of rainfall data). Cylindrical, sand-filled,

Table I. Mean soil properties of the road surface soil at PKEW

Descriptor/property	Units	*n*	PKEW Road[a]
Sand fraction	%	8	$54{\cdot}4 \pm 4{\cdot}9$
Silt fraction	%	8	$24{\cdot}0 \pm 2{\cdot}2$
Clay fraction	%	8	$21{\cdot}7 \pm 5{\cdot}5$
Dominant clay mineral	—	4	Kaolinite[b]
Saturated hydaulic conductivity	mm h^{-1}	26	$15{\cdot}0 \pm 8{\cdot}6$
Wetness at saturation (also saturated porosity)	m m^{-3}	26	$0{\cdot}44 \pm 0{\cdot}05$
Water retained at −330 kPa	m m^{-3}	5	$0{\cdot}30 \pm 0{\cdot}01$
Water retained at −1500 kPa	m m^{-3}	5	$0{\cdot}13 \pm 0{\cdot}01$
Preferential porosity	m m^{-3}	5	$0{\cdot}10 \pm 0{\cdot}03$
Bulk density (0–5 cm)	Mg m^{-3}	74	$1{\cdot}45 \pm 0{\cdot}13$
Bulk density (5–10 cm)	Mg m^{-3}	16	$1{\cdot}36 \pm 0{\cdot}11$
Bulk density (10–15 cm)	Mg m^{-3}	16	$1{\cdot}35 \pm 0{\cdot}10$
Penetration resistance	MPa	160	$6{\cdot}4 \pm 0{\cdot}4$
Particle density	Mg m^{-3}	8	$2{\cdot}55 \pm 0{\cdot}05$
$pH_{(1:5water)}$	—	16	$4{\cdot}8 \pm 0{\cdot}3$
Organic carbon	%	16	$1{\cdot}6 \pm 0{\cdot}6$
Total nitrogen	%	16	$0{\cdot}13 \pm 0{\cdot}03$
Cation exchange capacity	$cmol_c$ kg^{-1}	16	$9{\cdot}8 \pm 2{\cdot}6$
Exchangeable bases	%	16	$63{\cdot}1 \pm 19{\cdot}8$

[a] Values determined from 90 cm^3 surface cores; values are means ± one standard deviation.
[b] For PKEW soils in general; additionally, traces of illite, vermiculite, gibbsite, montmorillonite and chlorite are present.

geotextile bags (3·0 m × 0·2 m × 0·1 m) were arranged to form rectangular plots. Plot dimensions for ROAD and WET simulations were 3·75 × 0·85 m; 3·75 × 0·80 m for HILL simulations. The ROAD surface typically included one 0·15–0·30 m wide, incised (0·10–0·15 m) rut. The HILL plot surface areas were entirely rutted. At the base of all plots, geotextile bags were arranged such that runoff was funnelled into a shallow drainage trench. The 0·21 m^2 triangular area (in addition to plot areas above) at the base of each plot contributed both runoff and sediment. A V-shaped aluminium trough, inserted into the vertical trench wall, allowed event-based sampling. The trench face was treated with a 5 : 1 mixture of water and Soil Sement™ (an acrylic vinyl acetate polymer from Midwest Industrial Supply, Inc., OH) to prevent sediment detachment. The ROAD simulations were conducted for 60 min after time to runoff (TTRO); HILL simulations, 45 min after TTRO; and WET simulations, 10 min after TTRO. Rainfall was measured with manual gauges placed on the plot borders. Discharge was determined by filling a 525-mL bottle at 2·5- or 5-min intervals after TTRO. After settling, the supernatant was decanted, and discharge samples were oven-dried at 105 °C for 24 h to determine mass of material transported. Sample discharge volumes were reduced to account for the presence of sediment. Instantaneous concentrations (C_t) were calculated as sediment mass per corrected discharge volume. Instantaneous discharge (Q_t) and sediment output (S_t) values were adjusted to rates per unit area by dividing by sample filling time and plot area.

Soil physical property measurements

Soil physical properties in Table I were determined either 1 m upslope or downslope of the ROAD simulation plots. Surface bulk density (ρ_b) and subsurface bulk density (at 5 and 10 cm depths) were determined by sampling a 5-cm depth with a 90 cm^3 core, then oven drying for 24 h at 105 °C. Soil penetrability, a measure of the ease with which an object can be pushed or driven into the soil (cf. Bradford, 1986), was determined with a static Lang™ penetrometer. The penetrometer provides an index of normal strength, termed the penetration resistance (PR), for the upper soil surface, typically about

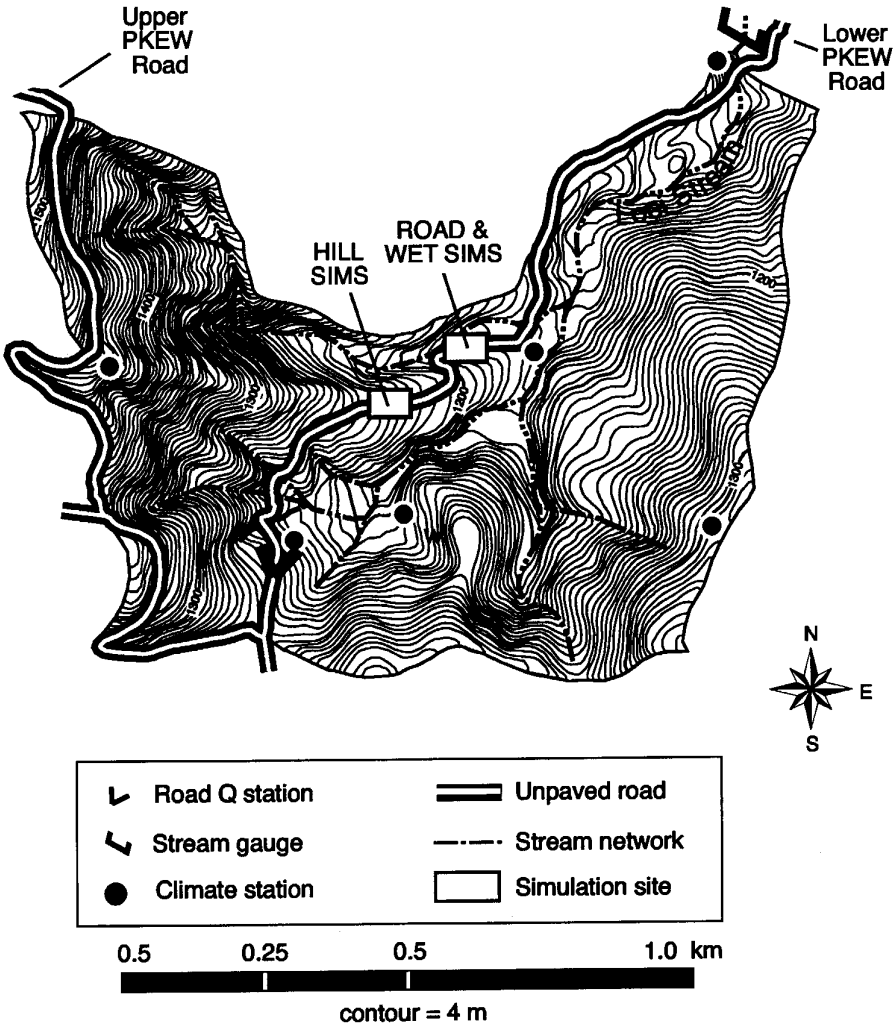

Figure 2. The 93·7 ha Pang Khum Experimental Watershed (PKEW). Field rainfall simulations were performed at two locations on the 1650 m section of the Lower PKEW Road bisecting the watershed

0·5 cm in depth—less on highly compacted surfaces, such as roads. Saturated hydraulic conductivity values were estimated from infiltration measurements taken *in situ* with Vadose Zone Equipment Corporation disk permeameters. Moisture retention data (soil moisture characteristic curves) were determined from 45 cm^3 cores collected from the road surface using standard procedures described in Klute (1986). Preferential porosity was computed as the difference in water content between $\psi = 0$ kPa (saturation) and that at -10 kPa. Measurements of cross-sectional physical characteristics and an inventory of sediment sources was performed on the Lower PKEW Road. A total of 32 cross-sections were established 50 m apart, beginning 25 m inside the watershed boundary. One suite of cross-sectional measurements was conducted in the dry season, March 1998; a second, 7 months later near the end of the wet season. At each cross-section, indices for the loose material were calculated from area-based gravimetric and volumetric calculations made of loose sediment collected with a brush and trowel from a 0·10 m swath across the road surface.

Model calibration and model error assessment

The ROAD simulation events 1, 2, 4, 5 and 7 were chosen randomly to produce a model calibration data set. Non-rectangular simulation plots were modelled in KINEROS2 as a singular rectangular element, having length and area equal to those in the field simulations; element widths were reduced to give equal areas. Median measured instantaneous and total runoff, sediment transport and sediment concentration values for the observed events (1, 2, 4, 5 and 7) were compared with those predicted by KINEROS2. Element parameters controlling runoff generation (e.g. capillary drive and K_s) and erosion processes (e.g. splash erosion and soil cohesion coefficients), which were assigned initially based on physical property data, were adjusted during calibration to reduce the error in predicted runoff and sediment transport. Five measures of model error or performance were used (Green and Stevenson, 1986; Loague and Green, 1991):

error in total estimate (%)
$$E_{\text{total}} = \frac{(P_{\text{total}} - O_{\text{total}})}{O_{\text{total}}} \times 100 \tag{8}$$

error in peak value estimate (%)
$$E_{\text{peak}} = \frac{(P_{\text{peak}} - O_{\text{peak}})}{O_{\text{peak}}} \times 100 \tag{9}$$

root mean square error (%)
$$RMSE = \sqrt{\frac{1}{n}\sum_{i=1}^{n}(P_{\text{i}} - O_{\text{i}})^2} \times \frac{100}{\overline{O}} \tag{10}$$

coefficient of determination
$$CD = \frac{\sum_{i=1}^{n}\left(O_{\text{i}} - \overline{O}\right)^2}{\sum_{i=1}^{n}\left(P_{\text{i}} - \overline{O}\right)^2} \tag{11}$$

model efficiency (ME, Nash and Sutcliffe, 1970)
$$R^2 = 1 - \frac{\sum_{i=1}^{n}(O_{\text{i}} - P_{\text{i}})^2}{\sum_{i=1}^{n}\left(O_{\text{i}} - \overline{O}\right)^2} \tag{12}$$

where P_{total} and O_{total} are event total predicted and observed values; P_{peak} and O_{peak} are peak event predicted and observed values; P_{i} and O_{i} are predicted and observed instantaneous values; and $\overline{O}$ is the mean of the observed data. If predicted and observed values are equal, E_{total}, E_{peak}, *RMSE*, *CD* and R^2 produce optimal values of 0, 0, 0, 1 and 1. Lower limits for E_{total}, E_{peak}, *RMSE* and *CD* are zero; model efficiency R^2 can be negative. The *CD* value indicates the proportion of total variance of observed data that is explained by the predicted data. A negative R^2 value indicates that model values are worse estimates than the observed mean (Loague and Green, 1991). Calibration first focused on reducing runoff E_{total} to $\pm 0{\cdot}5\%$; parameters where then adjusted to produce a better fit of the predicted runoff hydrograph, as indicated by the other performance indices (i.e. *RMSE*, *CD* and *ME*). The subsequent adjustments maintained an E_{total} of $\pm 0{\cdot}5\%$. Following runoff calibration, adjustments were made to splash and hydraulic detachment parameters to first reduce sediment transport total error to $\pm 0{\cdot}5\%$, then produce the best fit of modelled versus observed values, as defined by *RMSE*, *CD* and *ME*.

Model validation

Validation of the ROAD12457 parameter set (Table II) was performed on three data sets: (i) the three ROAD simulations not used for calibration (events 3, 6 and 8); (ii) the HILL simulations; and (iii) the WET simulations. The first data set allowed validation under initial conditions similar to those of ROAD12457. The HILL data set allowed validation on a steeper road section, with drier antecedent moisture conditions and greater surface sediment than ROAD12457. Surface preparation refers to events/phenomenon contributing to availability, detachment or entrainment of surface material (e.g. vehicular traffic, maintenance or mass wasting—cf. Ziegler *et al.*, in press). The WET data set allowed validation during typical wet season conditions: i.e., when high initial soil moisture content produces fast runoff generation, and prior HOF events

Table II. The ROAD12457 parameter set following calibration

Parameter[a]	Description	Value	Units	Calculation/estimation method
TH	Thickness of soil layer 1	0·15	m	Field examination of soil profile
$K_{s,1}$, $K_{s,2}$	Saturated hydraulic conductivity	4·05	mm h^{-1}	Reduced from Table I value during calibration
$C_v K_s$	Coefficient of variation for K_s	0·61	—	Table I
G_1	Layer 1 capillary drive	15	mm	Reduced during calibration from value in Rawls *et al*. (1982) for sandy clay loam.
G_2	Layer 2 capillary drive	36	mm	Same as for G_1
λ	Pore size distribution index	0·25	—	Rawls *et al*. (1982) for sandy clay loam
SAT	Initial relative saturation	0·47	—	Calculated as pre-storm soil wetness divided by wetness at saturation
ϕ_1, ϕ_2	Layer 1 and 2 porosity	0·43	cm^3 cm^{-3}	Estimated as soil wetness at saturation
c_f	Rain splash coefficient	261·6[b]	s m^{-1}	Determined during calibration from estimated value (Figure 4)
c_g	Soil cohesion coefficient	0·0196[b]	—	Same as for c_f
RELIEF	Average microtopographic relief	100	mm	Field measurements
SPACING	Average microtopographic spacing	0·40	m	Field measurements
ρ_s	Particle density	2·55	Mg m^{-3}	Table I
MAN	Manning's *n* roughness coefficient	0·015	—	Comparison of field conditions with values in Morgan (1995)
INT	Interception depth	0	mm	Field measurements
ROCK	Volumetric rock fraction of the soil column	1	%	Field measurements

[a] Subscripts refer to an upper (1) or lower (2) soil layer utilized by the infiltration subcomponent.
[b] For dynamic erosion (DE) modelling $c_f = 139·95$ and $c_g = 0·0105$.

have reduced loose surface sediment availability. One validation goal was to identify parameters sensitive to physical differences related to topography, soil moisture and surface preparation.

RESULTS

Model calibration

Table III lists rainfall intensity, storm duration, plot slope, an index of initial soil moisture (*SAT* in Table II), runoff (*RO*), total sediment output (*S*) and total sediment concentration (*C*) for rainfall simulation events modelled during KINEROS2 calibration and validation experiments. Events are referred to by simulation type (i.e. ROAD, HILL or WET) and one or a string of digits indicating a specific simulation number, or referring to the median values of several sites (e.g. ROAD368 refers to the median of ROAD simulations 3, 6 and 8).

Median instantaneous discharge (Q_t), sediment transport (S_t), and concentration (C_t) values for calibration event ROAD12457 are shown with KINEROS2-predicted values in Figure 3. Following parameter optimization, errors in predicted total *RO* and *S* were $\leq$0·5% (Tables IV and V). The Q_t time series is well-modelled by KINEROS2 ($RMSE = 14\%$; $CD \approx 0·80$; $R^2 = 0·84$); modelled peak discharge is underestimated by only $\approx$3% (Figure 3a). Substantially higher prediction error exists for instantaneous and peak S_t and C_t (Tables V and VI). The sediment peak in the first 20 min of the event, and the corresponding high C_t values, are not predicted by KINEROS2 (Figure 3b and c). The *RMSE* values for predicted *S* and *C* are >50 and 100%,

Table III. Summary of event characteristics and output for rainfall simulation experiments used for validation of KINEROS2

Simulation identity	Event/plot variables[a]				Total outputs		
	R_i (mm h^{-1})	Duration (min)	Slope (m m^{-1})	*SAT*	*RO* (mm)	*S* (kg)	*C* (kg m^{-3})
ROAD1[b]	91	61·2	0·14	0·54	75·7	5·0	16·7
ROAD2	110	60·8	0·14	0·53	98·4	6·2	16·0
ROAD3	94	61·5	0·13	0·40	72·2	5·6	19·7
ROAD4	107	61·4	0·13	0·26	95·2	9·4	24·9
ROAD5	100	61·2	0·14	0·47	84·1	4·4	13·2
ROAD6	116	60·6	0·18	0·43	95·0	5·4	14·3
ROAD7	108	61·2	0·18	0·41	91·5	13·5	37·3
ROAD8	112	60·9	0·17	0·38	96·1	4·6	12·1
ROAD12457	107	61·2	0·14	0·47	91·5	6·2	16·7
ROAD368	112	60·9	0·17	0·40	95·0	5·4	14·3
HILL1	108	46·6	0·24	0·25	61·2	13·3	57·5
HILL2	131	47·0	0·24	0·25	86·4	15·7	48·3
HILL3	92	46·4	0·29	0·27	56·7	17·0	79·6
HILL4	123	46·2	0·29	0·12	76·7	15·7	54·3
HILL	115	46·5	0·26	0·25	69·0	15·7	55·9
WET1	90	10·9	0·14	0·74	12·6	0·78	15·6
WET2	100	11·3	0·14	0·78	12·3	0·79	16·2
WET3	93	10·8	0·13	0·74	9·8	0·54	14·1
WET4	102	10·5	0·13	0·74	14·8	2·04	34·8
WET5	113	10·5	0·14	0·84	16·3	0·57	8·8
WET6	127	10·3	0·17	0·82	18·3	0·66	9·1
WET7	118	10·7	0·18	0·84	14·4	0·96	16·8
WET8	120	10·5	0·17	0·85	13·3	0·33	6·2
WET	108	10·6	0·14	0·80	13·9	0·72	14·8

[a] Duration = total simulation time; SAT is defined in Table II; *RO*, *S* and *C* are total runoff, sediment output and concentration.
[b] Digits refer to one specific simulation event; strings of digits indicate that values are medians of several events; HILL and WET refer to medians of all events of that type.

respectively; and S_t and C_t peaks are underestimated by >41 and 78%, respectively. Only during the middle third of ROAD12457 is S_t well-described by KINEROS2. Low E_{total} for KINEROS2-predicted *S* results from a balance of underprediction of S_t at the beginning of the event, and overprediction toward the end.

The ROAD12457 parameter set

The calibration stage produced a parameter set (ROAD12457) for use during model validation. In the ROAD12457 parameter set (Table II), the soil is described as a two-layer column, with the upper layer having thickness (*TH*) 0·15 m. Layer one depth was determined from field profile observations and bulk density measurements. Numeric subscripts in Table II refer to upper (1) and lower (2) soil layers, the latter for which depth is not specified. Our parameter specification approach initially used field-measured values. Changes having physical basis were then allowed to calibrate the discharge and sediment transport responses. For example, field-measured K_s (15·0 mm h^{-1}) was reduced to 4·1 mm h^{-1}, a value slightly less than the rainfall-simulation-derived estimate of steady state infiltration (5·4 mm h^{-1}). The original coefficient of variation for the K_s data was retained for C_vK_s. Values of G_1 and G_2 for the highly disturbed road surface were reduced by an order of magnitude during calibration from recommended values for sandy clay loam soils (Rawls *et al.*,

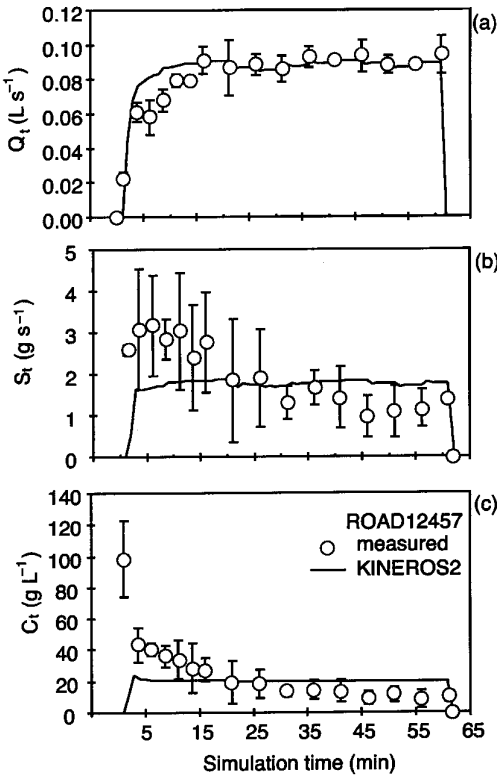

Figure 3. Comparison of (a) discharge, (b) sediment transport rate and (c) concentration between measured rainfall simulation data (circles) and KINEROS2-predicted values. Measured values are medians from ROAD events 1, 2, 4, 5 and 7; error bars are ± one median absolute deviation about the median. The KINEROS2 model was run using the calibration parameter set (Table II)

Table IV. Errors between observed and KINEROS2-predicted runoff

Simulation identity	Observed (mm)	Predicted (mm)	E_{total}[a] (%)	E_{peak} (%)	*RMSE* (%)	*CD* (r^2)	*ME* (R^2)
ROAD12457[b]	91·5	91·1	−0·47	−3·44	14·0	0·82	0·84
ROAD368	95·0	91·2	3·84	−2·22	23·4	0·80	0·65
ROAD3	72·2	80·9	12·03	−1·96	29·6	0·87	0·52
ROAD6	95·0	103·1	8·47	34·21	62·5	0·37	−1·15
ROAD8	96·2	100·0	4·02	−9·46	22·6	0·92	0·68
HILL	69·0	74·2	7·52	−1·11	17·6	0·79	0·81
WET	13·9	16·5	18·98	0·43	21·5	0·67	0·85

[a] E_{total} is error in total output estimate (Equation 8); E_{peak} is error in peak estimate (Equation 9); *RMSE* is root mean square error (Equation 10); *CD* is coefficient of determination (Equation 11); *ME* is model efficiency (Equation 12).
[b] Events modelled using dynamic erodibility method have same discharge values as event reported here.

1982). Pore size distribution index (λ) corresponds to that of sandy clay loam soil in Rawls *et al*. (1982). Initial soil saturation (SAT) was calculated as initial soil moisture divided by soil moisture at saturation (Table I).

Table V. Errors between observed and KINEROS2-predicted sediment output

Simulation identity	Observed (kg)	Predicted (kg)	E_{total}[a] (%)	E_{peak} (%)	*RMSE* (%)	*CD* (r^2)	*ME* (R^2)
ROAD12457	6·22	6·23	0·22	−41·2	51·6	1·64	0·77
ROAD368	5·39	7·92	46·8	−41·9	87·1	0·72	0·44
ROAD3	5·63	4·96	−11·9	−68·5	75·9	2·14	0·61
ROAD6	5·39	9·83	82·3	−26·3	117·9	0·76	0·09
ROAD8	4·63	8·88	92·1	−36·0	96·8	0·51	0·32
HILL	15·69	10·66	−32·1	−67·0	70·1	3·22	0·62
WET	0·72	1·25	73·4	56·2	84·0	0·34	0·38
ROAD12457 DE[b]	6·22	6·47	4·04	−3·93	35·4	1·11	0·89
HILL DE	15·69	14·64	−6·69	−21·9	44·6	0·97	0·85
ROAD3 DE	5·63	5·23	−7·07	−61·3	71·4	1·55	0·66
ROAD6 DE	5·39	8·07	49·6	−39·9	92·3	0·91	0·44
ROAD8 DE	4·63	6·84	48·0	−26·9	64·5	0·63	0·70

[a] E_{total} is error in total output estimate (Equation 8); E_{peak} is error in peak estimate (Equation 9); *RMSE* is root mean square error (Equation 10); *CD* is coefficient of determination (Equation 11); *ME* is model efficiency (Equation 12).
[b] DE refers to dynamic erodibility modelling method (Equation 13).

Table VI. Errors between observed and KINEROS2-predicted sediment concentration

Simulation identity	Observed (kg m^3)	Predicted (kg m^3)	E_{total}[a] (%)	E_{peak} (%)	*RMSE* (%)	*CD* (r^2)	*ME* (R^2)
ROAD12457	16·7	20·1	20·6	−78·4	104·8	3·05	0·38
ROAD368	14·3	25·5	78·3	−69·1	102·1	1·44	0·49
ROAD3	19·7	18·0	−8·36	−77·6	118·6	3·03	0·32
ROAD6	14·3	28·1	95·9	−82·7	154·9	3·68	0·23
ROAD8	12·1	26·1	115·2	−72·5	84·2	1·72	0·60
HILL	56·0	44·9	−19·7	−84·5	116·5	7·94	0·29
WET	14·8	22·3	50·4	51·6	88·4	0·45	0·35
ROAD12457 DE[b]	16·7	20·9	25·1	−64·7	97·0	2·04	0·47
HILL DE	56·0	61·7	10·3	−61·9	103·4	2·23	0·44
ROAD3 DE	19·7	19·0	−3·33	−67·2	113·3	2·09	0·38
ROAD6 DE	14·3	23·0	60·8	−76·9	141·5	3·24	0·36
ROAD8 DE	12·1	20·1	65·8	−63·0	62·8	1·88	0·78

[a] E_{total} is error in total output estimate (Equation 8); E_{peak} is error in peak estimate (Equation 9); *RMSE* is root mean squared error (Equation 10); *CD* is coefficient of determination (Equation 11); *ME* is model efficiency (Equation 12).
[b] DE refers to dynamic erodibility modelling method (Equation 13).

RELIEF refers to vertical changes in microtopography over the prescribed SPACING interval. Porosity (ϕ) and particle density (ρ_s) were determined from physical measurements (Table I).

First-guess values of c_f and c_g were assigned by solving Equations (6) and (7), respectively, using observed discharge, concentration and water depth data from a prior work (Ziegler *et al*., 2000a). Values of c_f and c_g were selected that produced the lowest *RMSE* between equation-predicted and observed splash and hydraulic erosion (Ziegler *et al*., 2000b) during the final 45 min of the ROAD rainfall simulation events 1, 2, 4, 5 and 7 (Figure 4). The initial 15-min period containing the flush of loose surface material was not included in the calculation, because we wanted the erodibilities to be that of the true road surface. The final values shown

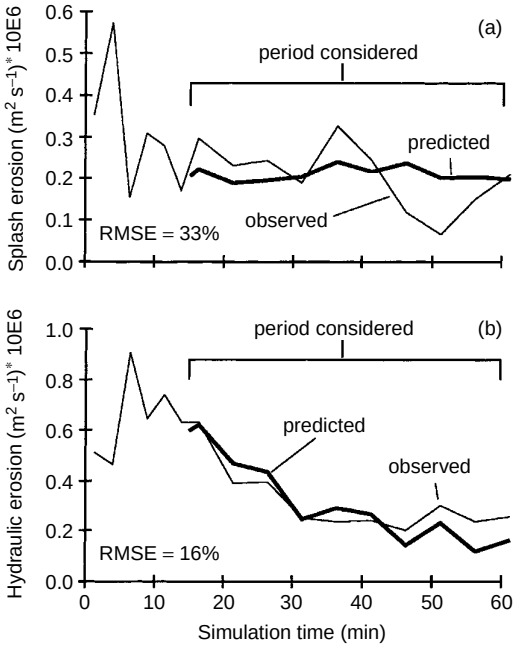

Figure 4. Comparison of (a) predicted splash (Equation 6) and (b) hydraulic (Equation 7) erosion that was measured during ROAD rainfall simulation events 1, 2, 4, 5 and 7. Coefficients c_f and c_g in Equations (6) and (7) were chosen to reduce the *RMSE* between predicted and observed values over the final 45 min of simulation, following the initial flush of loose material. These optimal values were then used as first-guess estimates for KINEROS2 c_f and c_g parameters prior to model calibration

in Table II were determined during model calibration by reducing the initial c_f and c_g values equivalently, to retain the proportionality between splash and hydraulic erosion.

ROAD validation

The results of the ROAD12457 parameter set validation using ROAD events 3, 6 and 8 are shown in Figures 5 and 6, and Tables IV–VI. Runoff was slightly overpredicted for all events and *RMSE* values were higher than those during calibration. During events 3 and 8, total variation in *RO* was better described than during ROAD12457 (e.g. $CD = 0{\cdot}87$ and $0{\cdot}92$, respectively). Event 6 was relatively poorly modelled, as indicated by comparatively high values for E_{peak} and *RMSE*, low *CD* and a negative value for model efficiency. Error values for the median ROAD368 event were reasonable. Total *RO* was overpredicted by only about 4%, E_{peak} was lower than during calibration and *CD* was nearly identical. The *RMSE* and R^2 values were worse for ROAD368 compared with ROAD12457 because of overprediction during the first 20 min of the ROAD368 simulation.

The KINEROS2 model overpredicted total sediment transport for ROAD368 by 47%, but underpredicted median peak values by ≈42% (Table V and Figure 6). For the individual events, E_{total} ranged from −12 to 92%, *RMSE* values were >75% and R^2 was as low as $0{\cdot}09$. Similar to the calibration simulations, overprediction of *S* resulted from the inability of KINEROS2 to predict the initial flush and subsequent decline in sediment output over time. Unlike the calibration phase, initial underprediction was not enough to compensate for overprediction at the end of the events. As a result, errors in predicted concentration values were generally high.

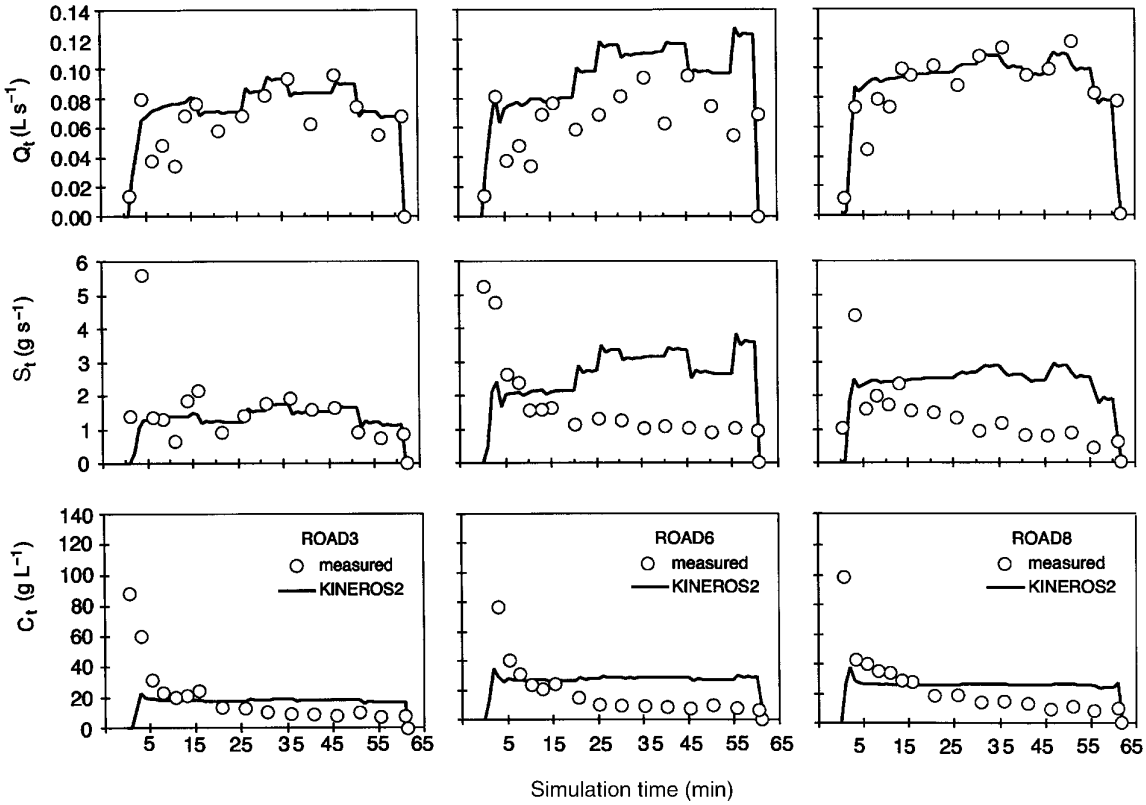

Figure 5. Comparison of discharge (Q_t), sediment transport rate (S_t) and concentration (C_t) between measured rainfall simulation data (circles) and KINEROS2-predicted values for ROAD events 3, 6 and 8. The KINEROS2 results were obtained using the calibration parameter set (Table II)

HILL validation

Simulation of the median HILL time-series using the ROAD12457 parameter set is shown in Figure 7. The discharge hydrograph was predicted reasonably, with $E_{\text{total}} = 7{\cdot}5\%$ and $RMSE \approx 18\%$ (Table IV). The *CD* and *ME* values for the predictions were only slightly lower than those during the ROAD12457 calibration. In contrast to overpredicting *S* during ROAD368 validation, KINEROS2 underpredicted sediment transport for HILL. Total error in *S* and *C* were $\approx -32\%$ and -20%, with much larger errors in peak estimates (Tables V and VI). The *RMSE* value for HILL-predicted *S* was ≈70%, but was smaller than that for ROAD368; *RMSE* in the *C* prediction was again greater than 100%.

WET validation

Wet validation results are shown in Figure 8 and Tables IV–VI. Predicted runoff was ≈19% higher than the observed median value. Much of this error results from overprediction during the first 5 min of this short event, for which there were few data points for evaluation of model performance. The error in peak output was less than 1%; and model efficiency R^2 was higher than that of the calibration event. Total sediment transport was overpredicted by ≈73% on this 'wet' surface, for which most loose sediment was removed during the previous day of simulation (Table V and Figure 8b). Model efficiency for the *S* prediction was the lowest of all median-based validation sets.

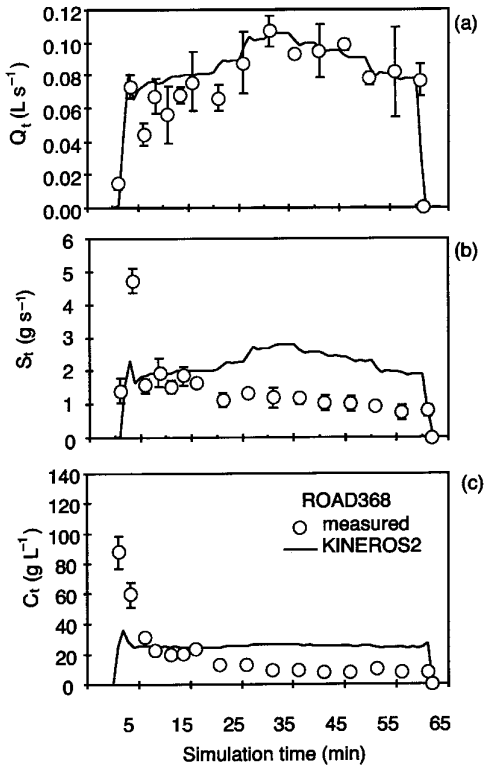

Figure 6. Comparison of (a) discharge, (b) sediment transport rate and (c) concentration between measured rainfall simulation data (circles) and KINEROS2-predicted values for ROAD368. Measured values are medians from ROAD events 3, 6 and 8; error bars are ± one median absolute deviation about the median. The KINEROS2 results were obtained using the calibration parameter set (Table II)

DISCUSSION

Soil moisture

Experimental conditions for ROAD368 were similar to those under which the calibration parameter set was produced. The HILL sites had greater slope and lower soil moisture content than the ROAD12457 site; and the WET sites had higher initial soil moisture (Table III). Runoff was well predicted in ROAD368 and HILL validation tests (E_{total} was within ±7·5%). Thus, KINEROS2 handled slope and soil moisture changes on these surfaces. Runoff during the WET validation was overpredicted by 19%. In comparison, the WEPP model used by Elliot *et al.* (1995) slightly overpredicted total event runoff values on 46·4 m^2 plots by 3–6% for dry, wet and very wet soil moisture conditions. Much of the model error for our WET simulations is related to the small time-series we have for the observed data during the 10-min rainfall simulations ($n = 5$ time stamps).

Sediment availability

Sediment transport was poorly predicted for ROAD368, HILL and WET events using the ROAD12457 calibration parameter set ($E_{\text{total}} = 47$, -32, and 73%, respectively). Although, underprediction of S for HILL could be related to higher erosive energy of hydraulic flow on the steeper slope, we believe the predominant cause for poor prediction at all sites is the difference in availability of loose surface material. During the ROAD12457 rainfall simulation experiments, most sediment removed up to some threshold value of total

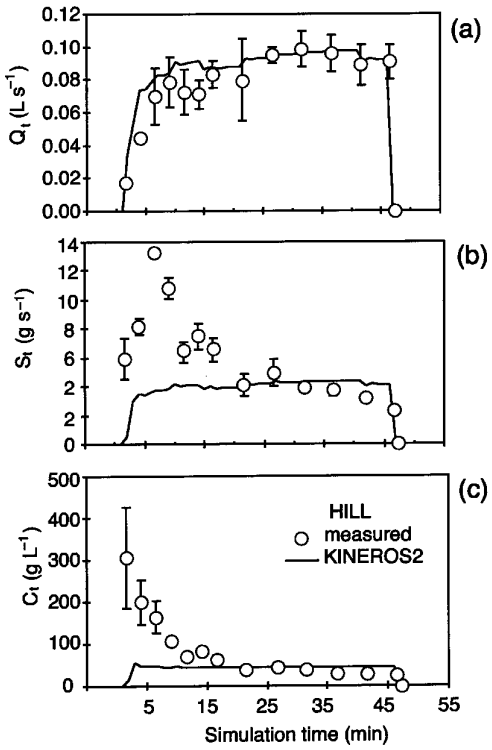

Figure 7. Comparison of (a) discharge, (b) sediment transport and (c) concentration between measured rainfall simulation data (circles) and KINEROS2-predicted values for the HILL validation. Measured values are medians from four HILL events; error bars are ± one median absolute deviation about the median. The KINEROS2 results were obtained using the calibration parameter set (Table II)

discharge was loose, previously detached material. In contrast, sediment output for the WET simulations was comparatively low because most loose material was removed on the previous day of rainfall simulation. The KINEROS2 model overpredicted *S* because the erosion parameters were determined for a road having a loose layer of surface material, i.e., the conditions for the ROAD simulations. Similarly, Elliot *et al*. (1995) reported that the WEPP model did not predict declines in erosion rates with successive storms.

The KINEROS2 model underpredicted *S* on HILL plots because these surfaces have more loose material than the ROAD12457 plots. Large quantities of loose surface material on the HILL plots result from higher vehicle-detachment rates on this comparatively steep surface. The sediment depth survey showed that the HILL road section contained three times more loose sediment than the ROAD plots (5·4 versus 1·8 kg m^{-2}). Total sediment transport for the HILL plots is best modelled by KINEROS2 using c_f and c_g values 3·55 times greater than those in the ROAD12457 calibration parameter set (not shown), suggesting that *S* is largely a function of sediment availability. Disparity in sediment transport between ROAD12457 and ROAD368 is related to high spatial variability in sediment depth on the road surface resulting from variability in interstorm preparation processes, including mass wasting, road maintenance and traffic.

Dynamic erodibility

In PKEW the road surface at any given time consists of a compacted, resilient surface underlying a layer of loose material of finite depth. Because the supply of road surface sediment is dynamic, road sediment transport response varies both during and between events. Sediment production is often high, such as following a long

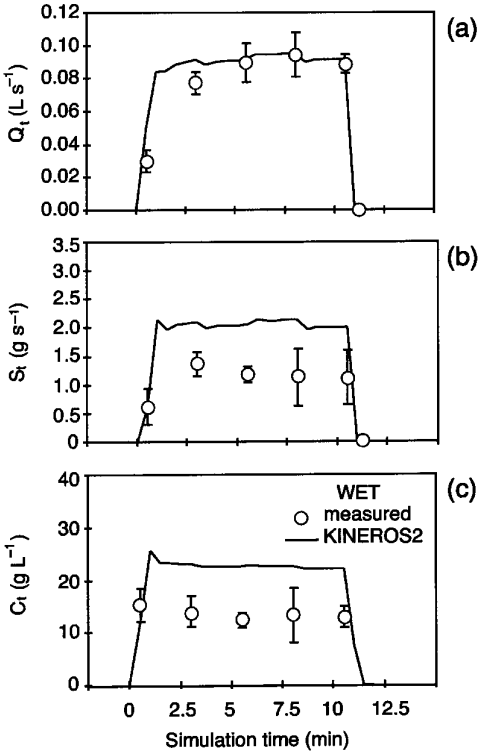

Figure 8. Comparison of (a) discharge, (b) sediment transport rate and (c) concentration between measured rainfall simulation data (circles) and KINEROS2-predicted values for the WET validation. Measured values are medians from eight WET events; error bars are ± one median absolute deviation about the median. The KINEROS2 results were obtained using the calibration parameter set (Table II)

dry period where traffic has generated a substantial layer of loose material. In general, roads receiving high traffic volumes tend to have high sediment production rates (cf. Reid and Dunne, 1984). Sediment transport is controlled initially by the ability of rain-affected surface flow to remove the loose surface layer, then by the ability to detach previously unavailable material from the compacted road surface. Both the underlying and loose material layers have unique erodibilities, with the loose layer generally being much more erodible. Thus, during a storm event, the road surface passes through two or more 'states' of erodibility. This dynamic erodibility can be represented by the following expression:

$$E_{\text{road}} = \begin{cases} E_2 & 0 \le d_{\text{cum}} \le c_2 d_{\text{s}} \\ E_1 & c_2 d_{\text{s}} \le d_{\text{cum}} \le c_1 d_{\text{s}} \\ E_0 & c_1 d_{\text{s}} < d_{\text{cum}} \end{cases} \tag{13}$$

where E_{road} is the dynamic erodibility (DE) of the composite road surface. For implementation in KINEROS2, E_{road} represents a scalar to multiply to baseline c_{f} and c_{g} erodibility parameters. The variable E_2 is the erodibility of the loose surface material at the start of a storm; E_0 is the baseline road erodibility of the compacted road surface; E_1 is an intermediate erodibility value after the initial flush of loose material; d_{s} is an index of sediment availability at the beginning of the storm (e.g. mass per area is used herein); c_1 and c_2 are values between 0 and 1; and d_{cum} is a value between 0 and d_{s} that represents cumulative removal of the surface material during a storm. The value of E_{road} at any time t is related to pre-storm sediment availability

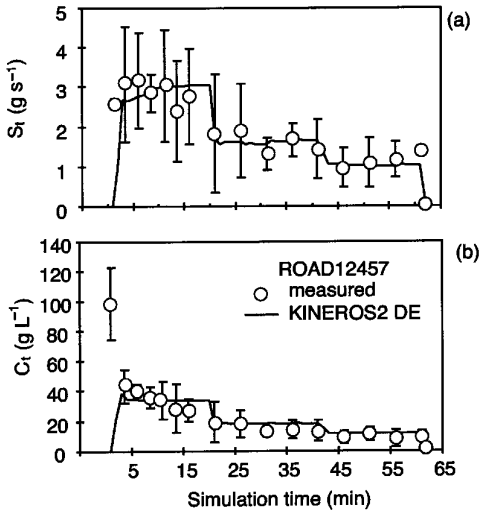

Figure 9. Modelling of (a) sediment transport rate and (b) concentration using the dynamic erodibility method (DE, Equation 13). Measured values are medians from ROAD rainfall simulation events 1, 2, 4, 5 and 7 (circles); error bars are ± one median absolute deviation about the median. The KINEROS2 results were obtained using the calibration parameter set, except c_f and c_g were 139·95 and 0·0105, respectively

(via d_s) and the amount of sediment thus far removed during the current modelled storm (d_{cum}). After d_{cum} surpasses thresholds defined by c_2 and c_1, E_{road} drops to that of a lower state. Implementation of the DE method requires empirical work to determine values for c_1, c_2, E_0, E_1 and E_2 for the modelled road. Sediment availability values, d_s, are also required for each storm modelled. As a modification to Equation (13), any number of erodibility states could be specified; ultimately, it could be represented as a continuous function.

Figure 9 shows calibration results for KINEROS2 modelling of ROAD12457 using the DE method. Values for E_0, E_1, E_2, d_s, c_1 and c_2 in Equation (13) were assigned as follows.

1. Baseline splash and hydraulic erodibility values for the underlying compacted road surface were established by optimizing KINEROS2 c_f and c_g parameters to minimize *RMSE* in predicted sediment transport for the 10-min WET simulations. Most loose material was removed from these plots during ROAD simulations on the previous day; therefore, we assumed WET sediment output resulted from detachment of new material from the compacted road surface. Optimization yielded values of 139·95 and 0·0105 for c_f and c_g, respectively.
2. Initial erodibility (i.e. the scalar $E_2 = 3{\cdot}4$) was determined by increasing baseline c_f and c_g values to reduce *RMSE* for sediment transport during the initial sediment output peak for ROAD12457 (i.e. roughly the first 15 min). Optimization during the period 20–40 min determined E_1 to be ≈0·5 E_2. Finally, $E_0 = 1$ (i.e. the baseline erodibility values).
3. Sediment availability (d_s) was assigned the value determined during the dry-season cross-section survey (1·8 kg m^{-2}). Sediment transport data for ROAD simulations 1, 2, 4, 5 and 7 suggested that the transitions between states E_2 and E_1, and then E_1 and E_0, occurred after ≈53% (c_2) and 84% (c_1) of the material, respectively, had been removed from the plots.

Using the DE method, *RMSE* for predicted *S* improved from 52 to 35% (Table V). Although total error increased slightly to 4%, compared with <0·5% error for the ROAD12457 calibration simulation, *CD* was reduced from 1·64 to 1·11; and *ME* (R^2) increased to 0·89, indicating that the DE-predicted values were better estimates of observed time-series than were the KINEROS2-predicted values. The improved estimates

of S produced better estimates of concentration; although, errors in the C estimate were still high, owing to poor estimation of the initial concentration spike following runoff generation. Temporal sediment response of ROAD12457 DE more closely describes the observed flush peak and the subsequent decline produced by the depletion of superficial material (Figure 9). Although more difficult to implement—because DE requires calibration and validation for all specified erodibilities—the dynamic erodibility method provides an improved approach for physically modelling removal of a loose road surface layer of finite depth. Figure 4 highlights the inability of Equation (6) to predict road splash response using observed discharge and water depth data. Predicted splash stabilizes after a few minutes because water depth, which is calculated as a function of runoff, stabilizes on the small-scale plots. Observed splash continues to decline because it is controlled by sediment availability, not increasing water depth, as modelled in Equation (6). The DE method addresses the change in sediment availability by modifying model parameters for erodibility.

Results from a second calibration of the DE modelling technique using HILL data are shown in Figure 10. Initial erodibility ($E_2 = 6{\cdot}1$) was determined by reducing *RMSE* of KINEROS2-predicted sediment transport during the initial flush of the HILL data. A value of $E_1 = 1{\cdot}9$ was determined by optimizing model erosion parameters during the middle 20 min of the HILL simulations. The sediment cross-section survey value of 5·4 kg m^{-2} was used for d_s. Similar to the ROAD12457 DE simulation, c_1 and c_2 were assigned values 53 and 84%, respectively. The KINEROS2-predicted values for HILL DE are shown in Figure 10. Simulation using the DE method substantially improved the 'goodness of fit' of the predicted S_t values: *RMSE* reduced from 70 to 45%, *CD* improved from 3·22 to 0·97, and model efficiency R^2 increased from 0·62 to 0·85. The *CD* value was the best of all simulations; and R^2 was second only to that of the ROAD12457 DE simulation.

General implementation of dynamic erodibility modelling

Using data from the ROAD12457 DE and HILL DE simulations, we developed a predictive relationship between road sediment depth and E_{road} values, which facilitates a general implementation of dynamic erodibility modelling using KINEROS2 (Figure 11). Initial erodibility, E_2, is determined from the amount of loose material present on the road surface at the beginning of an event. In Figure 11, this value is

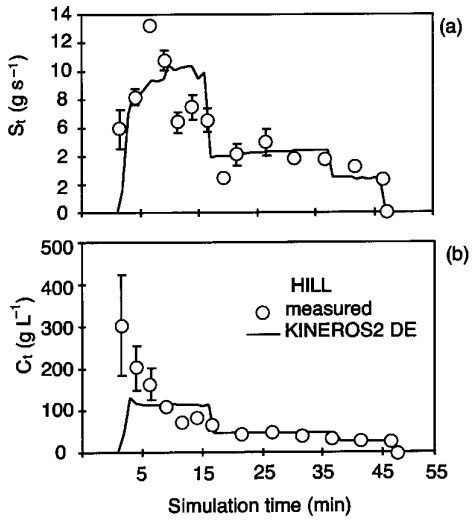

Figure 10. Modelling of (a) sediment transport rate and (b) concentration using the dynamic erodibility method (DE, Equation 13). Measured values are medians from all HILL rainfall simulation events (circles); error bars are ± one median absolute deviation about the median. The KINEROS2 results were obtained using the calibration parameter set, except c_f and c_g were 139·95 and 0·0105, respectively

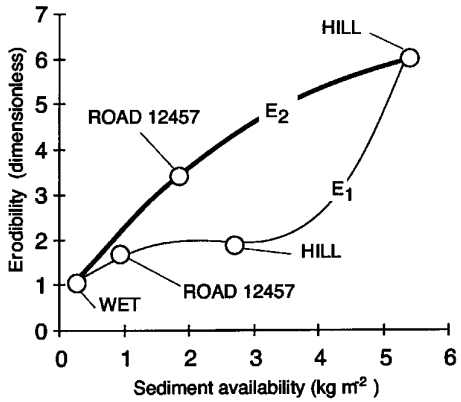

Figure 11. Relationship between surface sediment (mass per area) and erodibility values (E_1 and E_2) used to implement the dynamic erosion method (Equation 13)

represented by the thick line fitted through the values of E_2 used in the WET, ROAD12457 DE and HILL DE events reported above. The E_1 value is calculated based on the amount of sediment remaining after some percentage of the initial sediment supply has been removed from the road. The value of E_1 is determined by the thin lined fitted through values used in the WET, ROAD12457 DE and HILL DE simulation events. Two functions are required for determining E_1 and E_2 because the relationship between erodibility and sediment availability changes following the initial flush of material. Erodibility is initially high, as sediment transport is limited by the transport capacity of the flowing water. After the flush, entrainment becomes more difficult as material must be moved into defined flow channels from upslope sediment sources or detached from the road surface. Armouring occurs as material becomes 'lodged' in surface depressions, thereby reducing sediment output. For all DE events, baseline road erodibility, E_0, is 1. Values $c_2 = 53\%$ and $c_1 = 84\%$ can be used to define transition points between successive erodibility states, or they could be determined from empirical data. Although based on limited rainfall simulation data, the prediction functions in Figure 11 represent a systematic method for estimating E_{road} values using pre-storm estimates of road sediment depth.

Figure 12 shows results from modelling ROAD events 3, 6 and 8 using dynamic erodibility, with E_{road} values predicted from Figure 11. Table VII lists sediment depth estimates and corresponding E_2, E_1, and E_0 values for the three modelled events. Predicted values of S and C are shown with prediction errors in Tables V and VI. Predicted runoff for the DE event is the same as for the non-DE predictions (Table IV). The DE implementation greatly improved sediment production estimates for all three events. The E_{total} values for ROAD events 6 and 8 reduced from 82 and 92% to less than 50%. Improvements in *RMSE* and *ME* (R^2) indicate a better fit of modelled instantaneous values (Figure 12). In general, concentration estimates also improved, although error values remained high, owing to the inability to predict initially high S_t values. These high S_t and C_t values might be better predicted by adding another erodibility state to the general DE model. The overprediction of ending S_t values in ROAD6 and ROAD8 suggest that the baseline erodibility E_0 value may be too high.

We have multiplied both c_f and c_g by E_{road}. One could argue that, based on the poor fit of predicted to observed splash erosion values in Figure 4 (as compared with the good fit of the predicted hydraulic erosion values), only the splash parameter c_g need be multiplied by E_{road}. In a prior work (Ziegler *et al*., 2000b), however, we found the splash erosion subcomponent to be less than the hydraulic component at all times during the 60-min rainfall simulations on the Thailand road site. Adjusting only the c_g parameter herein would have violated this relationship. In other physical settings, unique scalar multipliers for c_f and c_g may be required.

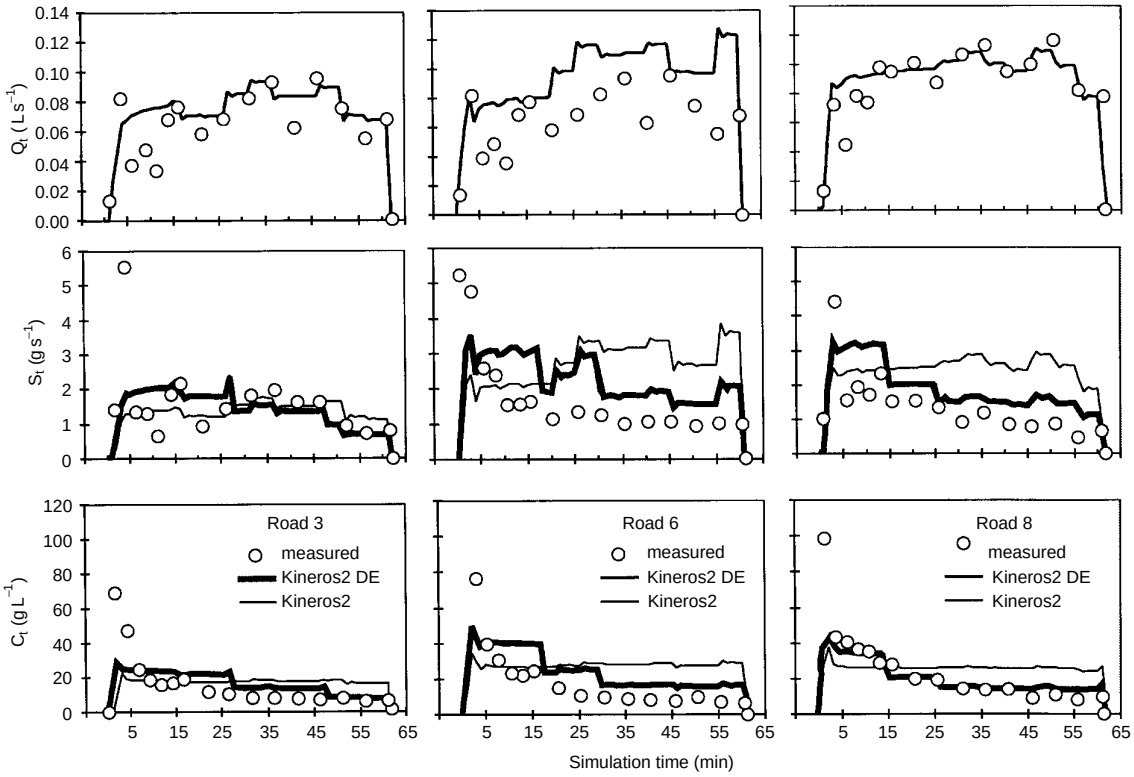

Figure 12. Modelling of discharge (Q_t), sediment transport rate (S_t), and concentration (C_t) using the dynamic erodibility method (DE, Equation 13). Measured values are for ROAD events 3, 6 and 8 (circles). The KINEROS2 DE results (thick line) were obtained using the calibration parameter set, except c_f and c_g were 139·95 and 0·0105, respectively. Results from standard KINEROS modelling are indicated by thin lines

Table VII. Parameter assignments for DE simulations

Simulation	d_s[a] (kg m^{-2})	E_2	E_1	E_0	c_2	c_1
ROAD12457 DE	1·80	3·60	1·70	1	0·53	0·84
HILL DE	5·40	6·10	1·90	1	0·53	0·84
ROAD3 DE	1·62	3·00	1·61	1	0·53	0·84
ROAD6 DE	1·56	3·14	1·69	1	0·53	0·84
ROAD8 DE	1·33	2·59	1·46	1	0·53	0·84

[a] Variables are defined in Equation 13.

SUMMARY

The KINEROS2 model can be parameterized to predict discharge hydrographs on small-scale plots under varying slope and soil moisture conditions. Temporal response in sediment transport on unpaved roads in the study area is best modelled when the superficial layer of loose sediment is considered explicitly. The dynamic erodibility approach introduced herein recognizes that roads have more than one state of erodibility, which

changes both between and during storm events. Initial road erodibility for any storm is related to availability of loose surface material, which is a function of interstorm sediment detachment processes. After removal of this upper layer, road erodibility is that of the compacted road surface itself. Using field rainfall simulation and KINEROS2 simulation data we developed a predictive relationship between sediment availability on the road surface and erosion parameter values needed to model erosion states. By implementing the DE method, we were able to better model sediment transport and concentration values observed during small-scale road rainfall simulation events. Our next step is to validate DE modelling at the hillslope scale, where runoff lag time and road surface water depth probably will be important mechanisms controlling discharge and sediment detachment.

ACKNOWLEDGEMENTS

Carl Unkrich, Southwest Watershed Research Center, USDA-ARS, Tuscon AZ (help with KINEROS2); Asuh, Atabuu, Atachichi, Aluong (brawn); K. Guntawong (the General); P. and N. Lamu (sharing their home), S. Yarnasarn, J. F. Maxwell (plant identification), and Jitti Pinthong (soil survey), Chiang Mai University; M. A. Nullet (engineering prowess), T. T. Vana (field assistance), Don Plondke (cartography), University of Hawaii; Yinglek Pongpayack, Sathaporn Jaiaree, and Sawasdee Boonchee, the Soil and Land Conservation Division of the Department of Land Development, Bangkok and Chiang Mai offices (soil analyses). This project was partially funded by a National Science Foundation Award (grant no. 9614259). Alan Ziegler was supported by an Environmental Protection Agency Star Fellowship and a Horton Hydrology Research Award (Hydrological Section, American Geophysical Union).

REFERENCES

Anderson DM, MacDonald LM. 1998. Modelling road surface sediment production using a vector geographic information system. *Earth Surface Processes and Landforms* **23**: 95–107.

Bradford JM. 1986. Penetrability. In *Methods of Soil Analysis, Part 1. Physical and Mineralogical Methods*, 2nd edn, Klute A (ed.). *Agronomy Monograph No. 9*, American Society of Agronomy–Soil Science Society of America: Madison, WI; 463–478.

Elliot WJ, Foltz RB, Luce CH. 1995. Validation of the water erosion prediction project (WEPP) model for low-volume forest roads. *Conference Proceedings 6, Sixth International Conference on Low-volume Roads*, Minneapolis, MN, 25–29 June. National Academy Press: Washington, DC; 178–186.

Flerchinger GN, Watts FJ. 1987. Predicting infiltration parameters for a road sediment model. *Transactions of the American Society of Agricultural Engineers* **30**(6): 1700–1705.

Grayson RB, Haydon SR, Jayasuriya MDA, Finlayson BL. 1993. Water quality in the mountainous ash forest: separating the impacts of roads from those of logging operations. *Journal of Hydrology* **150**: 459–480.

Green IRA, Stephenson D. 1986. Criteria for comparison of single event models. *Hydrological Sciences Journal* **31**: 395–411.

Klute A. 1986. Water retention: laboratory methods. In *Methods of Soil Analysis, Part 1. Physical and Mineralogical Methods*, 2nd edn, Klute A (ed.). *Agronomy Monograph No. 9*, American Society of Agronomy–Soil Science Society of America: Madison, WI; 636–662.

Loague K, Green RE. 1991. Statistical and graphical methods for evaluating solute transport models: overview and application. *Journal of Contaminant Hydrology* **7**: 51–73.

Luce CH, Cundy TW. 1994. Parameter identification for a runoff model for forest roads. *Water Resources Research* **30**: 1057–1069.

Megahan WF, Ketcheson GL. 1996. Predicting downslope travel of granitic sediments from forest roads in Idaho. *Water Resources Bulletin* **32**(2): 371–382.

Megahan WF, Kidd WJ. 1972. Effects of logging and logging roads on erosion and sediment depostition from steep terrain. *Journal of Forestry* **7**: 136–141.

Montgomery DR. 1994. Road surface drainage, channel initiation, and slope stability. *Water Resources Research* **30**: 1925–1932.

Morgan RPC. 1995. *Soil Erosion and Conservation*. Longman Group Limited: Harlow; 198.

Nash JE, Sutcliffe JV. 1970. River flow forecasting through conceptual models. Part I—a discussion of priniciples. *Journal of Hydrology* **10**: 282–290.

Rawls WJ, Brakensiek DL, Saxton KE. 1982. Estimation of soil water properties. *Transactions of the American Society of Agricultural Engineers* **2**(5): 1316–1320, 1328.

Reid LM. 1993. *Research and Cumulative Watershed Effects*. General Technical Report, PSW-GTR-141, US Department of Agriculture, Forest Service; Pacific SW Research Station, Albany CA 118.

Reid LM, Dunne T. 1984. Sediment production from forest road surfaces. *Water Resources Research* **20**: 1753–1761.

Simons DB, Li RM, Shiao LY. 1977. *Formulation of a Road Sediment Model. Report CER76-77DBS-RML-LYS50, Colorado State University: Fort Collins, CO; 107.*

Simons DB, Li RM, Ward TJ. 1978. Simple road sediment yield model. Report CER77-78DBS-RML-TJW-LYS41, Colorado State University: Fort Collins, CO; 70.

Smith RE. 1976. Field test of a distributed watershed erosion/sedimentation model. In *Soil Erosion, Prediction, and Control*. Special Publication 21, Soil Conservation Society of America: Ankeny, IA; 201–209.

Smith RE, Goodrich DC, Quinton JN. 1995. Dynamic, distributed simulation of watershed erosion: the KINEROS2 and EUROSEM models. *Journal of Soil and Water Conservation* **50**(5): 517–520.

Storck P, Bowling L, Wetherbee P, Lettenmaier D. 1998. Application of a GIS-based distributed hydrology model for prediction of forest harvest effects on peak stream flow in the Pacific Northwest. *Hydrological Processes* **12**: 889–904.

Ward TJ, Seiger AD. 1983. *Adaptation and Application of a Surface Erosion Model for New Mexico Forest Roadways. Technical Completion Report Project Nos 1423669 and 1345667, New Mexico Water Resources Research Institute, New Mexico State University: Las Cruces, NM; 83.*

Woolhiser DA, Smith RE, Goodrich DA. 1990. *KINEROS, a Kinematic Runoff and Erosion Model: Documentation and User Manual*. ARS-77, US Department of Agriculture, Agricultural Research Service; **25**(5): 519–534, 130.

Ziegler AD, Giambelluca TW. 1997a. Importance of rural roads as source areas for runoff in mountainous areas of northern Thailand. *Journal of Hydrology* **196**(1/4): 204–229.

Ziegler AD, Giambelluca TW. 1997b. Simulation of runoff and erosion on mountainous roads in northern Thailand: a first look. In *Human Impact on Erosion and Sedimentation*, Proceedings of Rabat Symposium S6, April, International Association of Hydrological Sciences Publication 245; 21–29.

Ziegler AD, Sutherland RA, Giambelluca TW. 2000a. Runoff generation and sediment transport on unpaved roads, paths, and agricultural land surfaces in northern Thailand. *Earth Surface Processes and Landforms*.

Ziegler AD, Sutherland RA, Giambelluca TW. In press. Interstorm surface preparation and sediment detachment by vehicle traffic on unpaved mountain roads. *Earth Surface Processes and Landforms*.

Ziegler AD, Sutherland RA, Giambelluca TW. 2000b. Partitioning total erosion on unpaved roads into splash and hydraulic components: the roles of inter-storm surface preparation and dynamic erodibility. *Water Resources Research* **34**(9): 2787–2791.

